Bioactive Materials 6 (2021) 2969–2982

Contents lists available at ScienceDirect

Bioactive Materials

journal homepage: www.sciencedirect.com/journal/bioactive-materials

Development of a polycaprolactone/poly(*p*-dioxanone) bioresorbable stent with mechanically self-reinforced structure for congenital heart disease treatment

Fan Zhao [a,b,d,1], Jing Sun [c,1], Wen Xue [a,b], Fujun Wang [a,b,**], Martin W. King [d], Chenglong Yu [a,b], Yongjie Jiao [a,b], Kun Sun [c,***], Lu Wang [a,b,*]

[a] College of Textiles, Donghua University, Shanghai, 201620, China
[b] Key Laboratory of Textile Science and Technology, Ministry of Education, College of Textiles, Donghua University, Songjiang District, Shanghai, 201620, China
[c] Department of Pediatric Cardiology, Xinhua Hospital, School of Medicine, Shanghai Jiao Tong University, No. 1665 Kongjiang Road, Shanghai, 200092, China
[d] Wilson College of Textiles, North Carolina State University, Raleigh, 27606, USA

ARTICLE INFO

Keywords:
Cardiovascular stent
Bioresorbable
Congenital heart disease
Braided technology
Thermal treatment

ABSTRACT

Recent progress in bioresorbable stents (BRSs) has provided a promising alternative for treating coronary artery disease. However, there is still lack of BRSs with satisfied compression and degradation performance for pediatric patients with congenital heart disease, leading to suboptimal therapy effects. Here, we developed a mechanically self-reinforced composite bioresorbable stent (cBRS) for congenital heart disease application. The cBRS consisted of poly(*p*-dioxanone) monofilaments and polycaprolactone/poly(*p*-dioxanone) core-shell composite yarns. Interlacing points in cBRS structure were partially bonded, offering the cBRS with significantly higher compression force compared to typical braids and remained good compliance. The suitable degradation profile of the cBRS can possibly preserve vascular remodeling and healing process. In addition, the controllable structural organization provides a method to customize the performance of the cBRS by altering the proportion of different components in the braids. The in vivo results suggested the cBRS supported the vessel wall similar to that of metallic stent. In both abdominal aorta and iliac artery of porcine, cBRS was entirely endothelialized within 1 month and maintained target vessels with good patency in the 12-month follow-up. The in vivo degradation profile of the cBRS is consistent with static degradation results in vitro. It is also demonstrated that there is minimal impact of pulsatile pressure of blood flow and variation of radial force on the degradation rate of the cBRS. Moreover, the lumen of cBRS implanted vessels were enlarged after 6 months, and significantly larger than the vessels implanted with metallic stent in 12 months.

1. Introduction

Congenital heart disease represents a major clinical problem worldwide because of the increasing incidences of myocardial ischemia, cardiac failure, and infective endocarditis [1]. It is considered as morphologic defects of the heart or great vessels in neonates or children. In clinic, suitable stents or scaffolds are required to prevent elastic recoil and intimal hyperplasia occurred in percutaneous transluminal angioplasty (PTA) [2]. Currently, drug-eluting stents (DES) are commonly used since they can reduce the in-stent acute restenosis and neo-intima tissue growth. However, the long-term adverse events of DES are reported such as delayed healing, neointimal hyperplasia, preventing late lumen expansion, and impairment of vessel geometries possibly due to their permanent metallic skeleton [3,4]. Besides, compared with adults,

Peer review under responsibility of KeAi Communications Co., Ltd.
* Corresponding author. College of Textiles, Donghua University, Shanghai, 201620, China.
** Corresponding author. Key Laboratory of Textile Science and Technology, Ministry of Education, College of Textiles, Donghua University, Songjiang District, Shanghai, 201620, China.
*** Corresponding author. Department of Pediatric Cardiology, Xinhua Hospital, School of Medicine, Shanghai Jiao Tong University, No. 1665 Kongjiang Road, Shanghai, 200092, China.
E-mail addresses: wangfujun@dhu.edu.cn (F. Wang), sunkun@xinhuamed.com.cn (K. Sun), wanglu@dhu.edu.cn (L. Wang).
[1] Fan Zhao and Jing Sun contributed equally to this work.

https://doi.org/10.1016/j.bioactmat.2021.02.017
Received 21 January 2021; Received in revised form 11 February 2021; Accepted 14 February 2021

whose vessel dimensions are fixed, the diameter of great vessels in infants and children can increase rapidly following their natural growth. In this case, permanent metal stents are no longer suitable. Bioresorbable stents (BRSs) emerge as a promising alternative to overcome those problems and satisfy the ever-increasing clinic needs [5]. BRSs provide temporary strength to support the pathological vessel at the expanded diameter and resist recoil before self-healing of vessels, whereby removing a permanent foreign body reaction [6].

Since bioresorbable polymers have good biocompatibility, adjustable degradation time, and good machinability, many types of polymeric bioresorbable stents were developed [7]. ABSORB BVS (Abbott Vascular) is the world's first clinically available polymeric bioresorbable stent (BRS), marked by CE in 2011 and granted FDA clearance in 2016 [8]. DESolve stent, DESolve 100 scaffold, developed by Elixir Medical (Milpitas, CA, USA) achieved CE marking in 2013 and 2014 [9]. Fantom, developed based on Reva stent, gained CE marking in 2017 [10]. Patients implanted with these stents have a certain beneficial effect in coronary artery treatment in short-term, comparative to those patients treated with DES [11]. However, the long-term efficacy of BVS was reported inferior to DES [11,12]. Studies have demonstrated the structural heterogeneities within BVS during fabrication and implantation (crimping and inflation), leading to localized deformation and asymmetric degradation [13]. In addition, the bioresorbable material used for BVS fabrication, poly-D,L-lactide, has a long absorption time in vivo (>2 years) [14], which mismatches with the vascular healing time (6–12 month). Thus, this stent was voluntarily withdrawn from sale in 2017. Other typical BRSs still lack randomized clinical data to evidence their therapeutic effect [15]. Currently, it is still a major challenge for typical BRSs to meet the structural and mechanical needs such as low crossing profile, low elastic recoil, and suitable degradation rate [5,16–19]. Furthermore, most of the available vascular BRSs aim to treat coronary artery diseases with small diameter of arteries from 3.5 mm to 5 mm. These BRSs implantation may fail to treat pediatric patients with congenital heart disease, due to the mismatch in the size of these stents with diseased great vessels (6–9 mm in diameter) [20,21]. Besides, simply enlarge the diameter of these typical BRSs cannot be succeeded, since higher mechanical demands are required for supporting great vessel than coronary artery. Hence, it is essential to develop a well-structured BRS with a larger diameter, sufficient strength and ideal degradation process to preserve long-term efficacy specific for pediatric patients.

To improve the performance of polymeric BRSs, we have previously developed a tri-axial braided stent prototype using PPDO monofilaments (diameter of 8 mm). It performed mechanically reinforced properties and acceptable degradation rate. This prototype is expected to enhance the compression resistance to support vascular lumen and it can be absorbed once vascular healing process completed [22]. However, the implantation of this stent in animal study was beset by its large crossing profile and poor flexibility, failed in the stent-delivery process. These challenges can also lead to immediate injury to the arterial wall, triggering smooth muscle cell responses from the media. Additionally, the bulk degradation of polymeric BRSs yields a large number of acidic degradation products, leading to local inflammatory response aggravation [18,19]. Thus, it is necessary to explore a new alternative with low crossing profile, good flexibility, and minimal inflammation response during polymeric BRS degradation.

In the present study, we developed a braided composite bioresorbable stent (cBRS) consisting of poly(*p*-dioxanone) (PPDO) monofilaments and polycaprolactone/poly(*p*-dioxanone) (PCL/PPDO) core-shell composite yarns. Partial crossing points of the cBRS structure were bonded after thermal treatment due to the difference of melt-points between PPDO and PCL. When it suffers from external radial force, the slippage and rotation of crossing yarns can be partially restricted and larger deformation is performed than typical braids. We hypothesis the braided cBRS has self-reinforced mechanical resistance with minimal increased crossing profile, good compliance and ideal degradation properties, thus it can maintain long-term vascular patency after stent implantation. To achieve this goal, the fabrication parameters of the cBRS were firstly investigated to get regular and stable structure. Then, the mechanical and in vitro degradation properties of the cBRS were evaluated. Biocompatibility was also evaluated by hemolysis and cell viability tests in vitro. Finally, the in vivo efficacy of the braided cBRS was studied by swine model.

2. Materials and methods

2.1. Materials

Poly(*p*-dioxanone) (PPDO) monofilaments and polycaprolactone (PCL) multifilament were used in this study to fabricate the braided cBRS due to their good biocompatibility and suitable degradation rate. They were dawn and stretched by melting spinning at Donghua University, Shanghai, China.

2.2. Finite element analysis

Stress distribution and deformation mechanism of different stent models were obtained by finite element analysis. Both stent models and parallel plates were constructed with Solidworks software (Verstion 2012). Braided stent models were designed with or without crossing-point fixation. They were then meshed with linear exanedron (C3D8) and linear reduced hexanedron element models respectively in Abaqus software (Version 6.14), which was offered with lengths of 0.3 and 1 mm according to a mesh convergence study. Neo-Hookean material [23] was used for the stent models according to the axial tensile test of stent yarns. The interaction of two crossing and unfixed yarns was set as a penalty function [24], with a friction coefficient of 0.25. While the "tie" constrains were applied on the crossing yarns with fixed crossing points. During the simulation, the two plates were fixed in all dimensions except the Y-axis displacement applied to the upper plate [25].

2.3. Fabrication of the PCL/PPDO core-shell braided yarn

PCL/PPDO core-shell braided yarns were fabricated on an 8-bobbin braiding machine at Donghua University. PPDO monofilament was wrapped by four groups of PCL multifilament, where PPDO was introduced from the center of the machine. PCL was arranged with diamond distribution on the bobbin. By optimizing the process conditions, evenly and entirely covered composite braided yarns can be obtained, and as thin as possible.

2.4. Fabrication of braided composite bioresorbable stents (cBRSs)

Our preliminary test showed the composite braided stents were rigid and lack of flexibility when they comprised by core-shell braided yarns only. Thus, the strategy of combining PPDO monofilaments with core-shell braided yarns was adopted to fabricate PCL/PPDO braided cBRSs. By changing the ratio of core-shell braided yarns and PPDO, two types of cBRSs were fabricated on a 32-bobbin braiding machine in the Biomedical Textile Materials Research Laboratory of Donghua University, Shanghai, China. In addition, typical stents braided by 32 PPDO monofilaments were used as control. All stents were braided with the same braiding angle and structure (regular braiding) and wrapped on the surface of a copper mandrel (outer diameter with 8 mm) to guarantee the uniformed inner diameter of stents. Thereafter, the holding fixture with the braided stents was placed in an electrothermal blowing dryer (Shanghai Yiheng Co., Ltd, China) for thermal treatment under 90 °C for 1 h. The core layer of braided yarns melted under thermal treatment due to low melting points of PCL. After cooling, the crossed core-shell melted yarns bonded together and formed the final cBRSs.

2.5. Measurement of PCL/PPDO core-shell melted yarn

The core-shell braided yarns formed by PPDO and PCL were transferred to core-shell melted yarns after thermal treatment due to soften and melt of PCL multifilament. According to the stent design, it is important to obtain the core-shell melted yarns entirely and evenly, and as thin as possible. High peeling strength of the bonded points of core-shell yarns are also required to remain stent structural stability. Thus, morphology and various mechanical properties of core-shell melted yarns were evaluated and compared with core-shell braided yarns and PPDO monofilaments.

2.5.1. Morphology

Morphology of core-shell yarns before and after thermal treatment was measured by using an optical microscope (Hitachi, Model S-4800, Japan).

2.5.2. Uniaxial tensile

Uniaxial tensile properties of core-shell yarns were measured and tensil load-elongation curves were obtained by using YG (B) 026G-500 universal testing system instrument (Wenzhou Darong Textile Instrument Co., Ltd., Wenzhou, China), respectively. The initial gauge length was 250 mm, and the velocity was 500 mm/min. Moreover, two core-shell braided yarns were crossed manually. After thermal treatment, the crossing points were bonded, which can mimic their position and status in the cBRS structure. The peeling force of two bonded core-shell melted yarns was measured by YG (B) 026G-500 universal testing system instrument with an initial gauge length of 100 mm and a velocity of 10 mm/min.

2.5.3. Bending rigidity

Bending rigidity of PPDO monofilaments, core-shell braided yarns, and core-shell melted yarns were tested by a bending tester (KES-FB2, KATO TEKKO CO., LTD, Japan) as reported by Conger et al. [26].

2.5.4. Friction force

Since yarns in the regular braiding structure were restricted by friction, the values between different yarns (PPDO monofilament, core-shell melted yarn) were measured by using an XF-1A friction tester (Shanghai New Yarn Instrument Co., Ltd., Shanghai, China). Each end was equally weight-loaded and the central yarn was dragged vertically with a velocity of 60 mm/min. By changing the vertical yarn from PPDO monofilament to core-shell melted yarn, the maximum static friction force and average dynamic friction force of PPDO filaments and core-shell melted yarns were recorded, respectively [27].

2.6. Measurement of the mechanical properties of braided cBRSs

2.6.1. Parallel compression measurement

The compression performance of cBRSs was investigated by using a customized parallel plate tester (Model LLY-06D, Lanzhou, Co., Ltd., China) according to ISO 25539-2012. cBRSs and the typical braids were compressed to 50% of their outer diameters and kept for 30s subsequently. The compression load-displacement curves were obtained (Supplementary Fig. 1), compression force was read and calculated accordingly. Then, the external load was removed gradually. After 30s, the plate touched the stent again. Therefore, the recovery load-displacement curve was recorded and the recovery rate could be calculated accordingly. Combining the two curves, the energy loss of stents during the loading and unloading process can also be calculated [25].

2.6.2. Compliance measurement

The compliance test of the composite bioresorbable stents was conducted by a BOSE dynamic simulated system (Model 100451, Bose Corporation, Framingham, MA). Test conditions were set as 1 Hz in test frequency, 80 mm Hg to 120 mmHg in pulsatile pressure, 100 mL/min in liquid flow rate, and deionized water as the test media. PU graft, a tubular membrane, is used as the positive control (provided by Bose Corporation, Framingham, MA), with inner diameter of 8 mm and thickness of 0.23 ± 0.01 mm. The outer diameter and pulsatile pressure were recorded during the test period and compliance (C) was calculated according to the following equation [28]:

$$C = \frac{\left(D_{p_2} - D_{p_1}\right)/D_{p_1}}{p_2 - p_1} \times 10^4$$

Where p_1 and p_2 are the lower and higher-pressure value (mmHg), respectively, D_{p_1} and D_{p_2} are the diameter of lower and higher pressure accordingly.

2.7. In vitro accelerated degradation test

Stents were placed unconstrained individually in plastic vials filled with phosphate-buffered saline (PBS, pH 7.4). The vials were placed in a water bath at 50 °C. The morphological and mechanical changes of stents at designed time points were measured and the degradation tests were terminated once the stents lost their mechanical resistance completely.

2.8. In vitro biological evaluation

2.8.1. Hemolysis measurement

Hemocompatibility was conducted by using fresh rabbit whole blood, which was obtained from male New Zealand rabbits by using a vacuum tube containing sodium citrate at a ratio of 9:1. After centrifuging the citrated blood for 5 min at 5000 rpm, 1 mL stable clot were hemolyzed by 34 mL phosphate-buffered saline (PBS) and collected as the red blood cells (RBC). Samples were immersed in 1 mL RBC and incubated for 2 h at 37 °C after added with 4 mL PBS. The solutions were centrifuged for 3 min for 5000 rpm and the supernatant was evaluated at 540 nm by a microplate reader (Tecan, Australia). 1 mL RBC mixed with 4 mL double distilled water and 1 mL RBC mixed with 4 mL PBS were served as positive control and negative control, respectively. The hemolysis rate is calculated by the following equation:

$$R = \frac{A - C_1}{C_2 - C_1} \times 100\%$$

Where: R is the hemolysis rate, A represents the absorbance of the samples, C_1 and C_2 are the absorbance of the negative and positive controls, respectively.

2.8.2. Cell viability measurement

The extraction method was used to evaluate the cell cytotoxic of composite bioresorbable stents. The pig iliac endothelium cell lines (PIEC suspension, purchased from the Cell Bank of the Chinese Academy of Sciences, Shanghai, China) were incubated in 88% (v/v%) Roswell Park Memorial Institute (RPMI), supplemented with 10% (v/v%) fetal bovine serum, 1% (v/v%) penicillin-streptomycin (Gibco), and 1% (v/v %) sodium pyruvate in the 5% CO_2 incubator at 37 °C. After sterilized by 75% ethanol and rinsed by PBS, samples (typical braids, cBRS-A, and cBRS-B) with the weight of 0.4 g were immersed in DMEM at an incubator for 24 h to obtain extraction media. Then, cells were seeded at a density of 5000 cells/well on 96-well plate and cultured with 100 μL extraction media. Before the cell viability was evaluated (1, 3, and 5 days), 40 μL Cell Count Kit-8 (CCK-8, Keygen) was added to each well and cultured for 4 h. Then, the optical density at 450 nm (OD 450) was measured by a microplate reader (Tecan, Australia).

2.9. Preclinical assessment

In vivo functionality of the cBRS was studied in swine artery models.

The protocol and experiments in this study is in accordance with accepted institutional policies, with the proof of the Animal Ethics Committee. 24 cBRS-A (diameter (D): 8 mm, length (L): 20 mm) and 12 commercial self-expanding metallic stent (Wallstents, (D: 8 mm, L: 21 mm)) were deployed in either iliac arteries or abdominal aortas of 20 miniature swine weighting 20–25 kg. For group one, 12 cBRSs were implanted in abdominal aortas. For group two, 12 cBRSs were implanted in iliac arteries. 12 Wallstetns were implanted in iliac arteries as the control group. Upon loading, the stent was crimped using a compression station, and an 8Fr delivery sheath was advanced over it due to its larger profile than metallic stents [29], just prior to implantation. The delivery system (AMPLATZER™ TorqVue 45 ° × 45 °, AGA Medical Corporation, USA) assembly was advanced over the 0.018 guild wire to the determined location either in one common iliac artery (CIA) or the aorta. Depending on the size of vessel where the stent landed, a post-dilation with an 8.0 mm balloon (Sterling Monorail PTA Balloon Dilatation Catheter, Boston Scientific Corporation, USA) was employed at the nominal pressure of 6 atm to obtain a better expansion of the braided stent and potentially reduce stent thrombosis. Wallstents were implanted by using 5 Fr catheter based delivery system with post-ballooning. The targeted vessel diameters were measured by angiography before and after stent implantation immediately and compared with vessels implanted with Wallstent. After stent implantation for 1, 4, 6, 12 months, angiography was conducted. The vessel diameter with or without stent implantation and lumen acquisition were assessed by using image measurement software (Syngo fastView , Version VX57H31). Luminal gain or loss was calculated as following equation:

$$\text{Luminal gain or luminal loss } \% = (\text{LD}_{\text{SV}} - \text{LD}_{\text{NSV}})100\%$$

Where: LD_{SV} means lumen diameter in the stented segment of vessel, LD_{NSV} represents non-stented segment of vessel.

Then swine models were sacrificed and cBRSs were harvested and preserved in formalin, dehydrated, and embedded in paraffin. The endothelialization of cBRSs was assessed by SEM images and the semi-quantitative scoring scheme for injury and inflammation was described. The cross-section of the stent was cut using a microtome and stained with hematoxylin and eosin for histopathological evaluation. Neointimal thickness (NT), external elastic lamina area (EELA), internal elastic lamina area (IELA), and luminal area (LA), neointimal area were measured. The histomorphometric area stenosis (AS) was calculated with the following equation:

$$AS\% = (IELA - LA) / IELA \times 100\%$$

Vessel injury and inflammation were rated on a scale of 0–3 according to previously reported methods [30]. Degradation degree of cBRSs was scored using method described by Hedberg et al. [31].

2.10. Statistic treatment

Students' t-tests were used for determining the statistical difference between samples. The data reported were the means and standard deviations, and the error bars in the figures corresponded to standard deviations. The data in the figures were marked by * for $p < 0.05$, ** for $p < 0.01$ and *** for $p < 0.005$.

3. Results

3.1. Design principle of braided cBRSs

We hypothesis that the braided cBRS is formed by two parts, as illustrated in Fig. 1a. The major part is formed by PPDO filaments. The physical restriction (friction force) of two contacted PPDO filaments can be easily breakthrough when suffered from external force and result in filaments slippage and rotation. This offers the braided stents good flexibility. Composite filaments serve as another part, which consist of PPDO and PCL. The crossing points of two composite filaments are bonded, which limits the movement of filaments at the bonding region. This part offers novel braided stents with superior mechanical resistance under external force compared to typical braids.

Three-dimensional finite element analysis can provide insight into the mechanics of compression resistance using the built models with crossing point fixations (CPF) partially [32]. Herein, it was used to verify this principle. The Von Mise stress distributions of stent models with or without crossing point fixation appear in Fig. 1b. Longitudinal elongation was limited in stent model with CPF, leading to incremental crossing points per unit during compression. Besides, the braiding angles kept unaltered during compression, resulted in yarns bending greatly and stress concentration zones emerging near the bonding points. Hence, stronger resistance obtained by the stent with CPF, compared with the control stent.

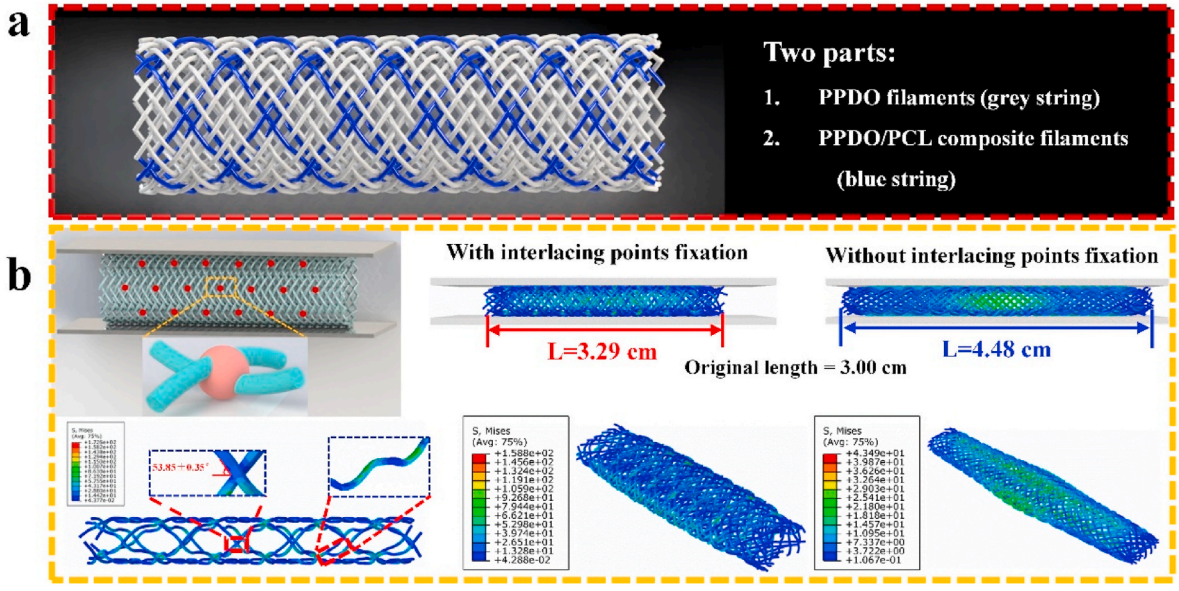

Fig. 1. a. Schematic representation of braided composite stent structure. b. Finite-element analysis results for the Von Mise stress distribution of braided stent models under parallel compression.

Herein, to impart wished composite filaments to the braided stents, we wrapped groups of PCL multifilament on the outer surface of PPDO monofilament. After introduced into braiding structure, the core-shell composite yarns interlaced with each other regularly. Under suitable thermal temperature, PCL layer was softened and its molecular chains moved and glided mutually at interlacing points while spread evenly in the outer surface of PPDO at other regions. So, the interlacing points were constrained and PPDO monofilaments were coated by a layer of PCL film after being cooled sufficiently. Besides, the good elasticity and extensibility of the PCL layer offered a strong binding force at the crossing points. It guarantees the structural stability of novel braided stents during compression and yields robust mechanical resistance.

3.2. Fabrication and structure evaluation of braided cBRSs

Fig. 2 explained the fabrication steps, beginning with the formation of PCL/PPDO core-shell braided yarns via an 8-bobbin braiding machine. By optimizing the process conditions, evenly and entirely covered composite braided yarns can be obtained (Fig. 2a, step 1). The fixation principle of crossing points was derived from thermally bonding process [27]. The uniaxial tensile results showed a two-stage tensile failure in the tensile load-displacement curve of core-shell braided yarns, suggesting the unstable combination of the two components. However, after PCL layer melted on the surface of PPDO, the two components yielded good binding strength with each other and contacted tightly during the entire tensile process (Fig. 2b). The bending rigidity of core-shell melted yarns showed 192.75% higher than that of PPDO monofilaments (4.69 ± 0.66 mN) (Fig. 2c). Moreover, the peeling force of the bonded core-shell melted yarns was 2126.67 ± 133.14 mN, 30-fold higher than the friction forces between two PPDO monofilaments (50.21 ± 5.23 mN) and between a PPDO monofilament and a composite melted yarn (63.37 ± 7.37 mN) (Fig. 2d). This indicates that the peeling force plays an important role in restricting the movement of braiding yarns in the cBRS structure.

The PCL/PPDO core-shell braided yarns were then arranged every three or seven PPDO monofilaments on a 32-bobbin braiding machine (Fig. 3a, step 2) to form composite stents preforms, cBRS-A preform, and cBRS-B preform, respectively (Fig. 3b). The two types of preforms tensioned and fixed on the copper mandrel were then thermally treated to get the final composite stents (Fig. 3c, step 3). Based on the difference of melting temperatures of PPDO and PCL yarns (102.73±0.15 °C and 56.03±0.21 °C, respectively), 90 °C 1 h were selected to heat-set the braiding structure and soften PCL layer in core-shell yarns [33,34]. Besides, an average cooling rate of 0.1 °C/min was adopted to increase crystallization integrity and structural stability.

The photograph of representative stents, with an inner diameter of 8 mm, was presented in Fig. 3c. Three interlacing modes, PPDO monofilament - PPDO monofilament, PPDO monofilament - core-shell composite yarn, and core-shell composite yarn - core-shell composite yarn, formed the crossing points in the cBRSs, as shown in the SEM images (Fig. 3d). The physical parameters of PCL/PPDO composite braided stents were shown in Table 1. The proportions of different interlacing modes among the braiding structure and the ratio of two components were calculated (Table 2 and Table 3). 2.21% (cBRS-A) and 8.33% (cBRS-B) crossing points were bonded in the cBRSs structure, and PCL component accounted for 11.6% and 20.87% (v/v%) of cBRS-A and cBRS-B respectively. This may offer composite braided stents with high compression resistance while good flexibility and compliance.

3.3. Mechanical characteristics of braided cBRSs

Compression resistance, including compression force and recovery performance, is a major challenge for polymeric stents, especially for braided stents [35]. Compression modulus of braided stents increased from 1184.03 ± 98.33 mN/mm (typical braids) to 1520.97 ± 113.58 mN/mm (cBRS-B). Compression forces of cBRS-A and cBRS-B enhanced

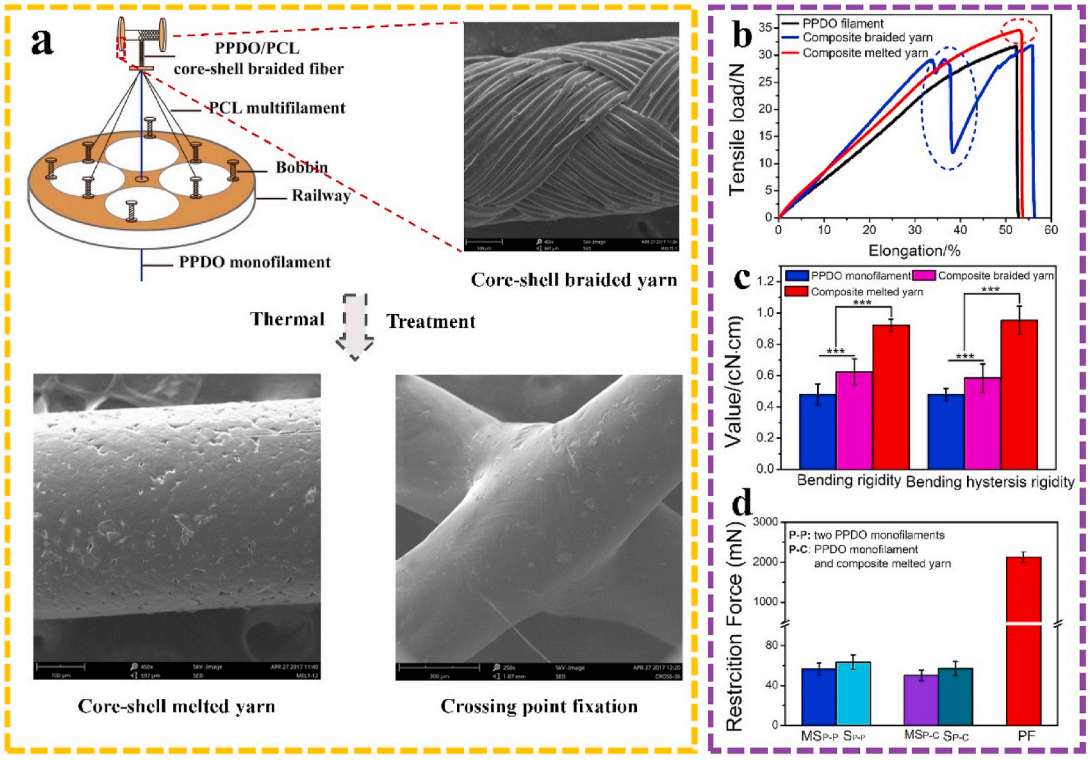

Fig. 2. a. Fabrication of PCL/PPDO core-shell braided yarns and core-shell melted yarns. b. Uniaxial tensile properties of PPDO monofilament, PCL/PPDO core-shell braided yarns and core-shell melted yarns. c. Bending rigidity of PPDO monofilament, PCL/PPDO core-shell braided yarns and core-shell melted yarns (n = 3, ***p < 0.005). d. Friction force and peeling force of different interlacing monofilaments or yarns (n = 3).

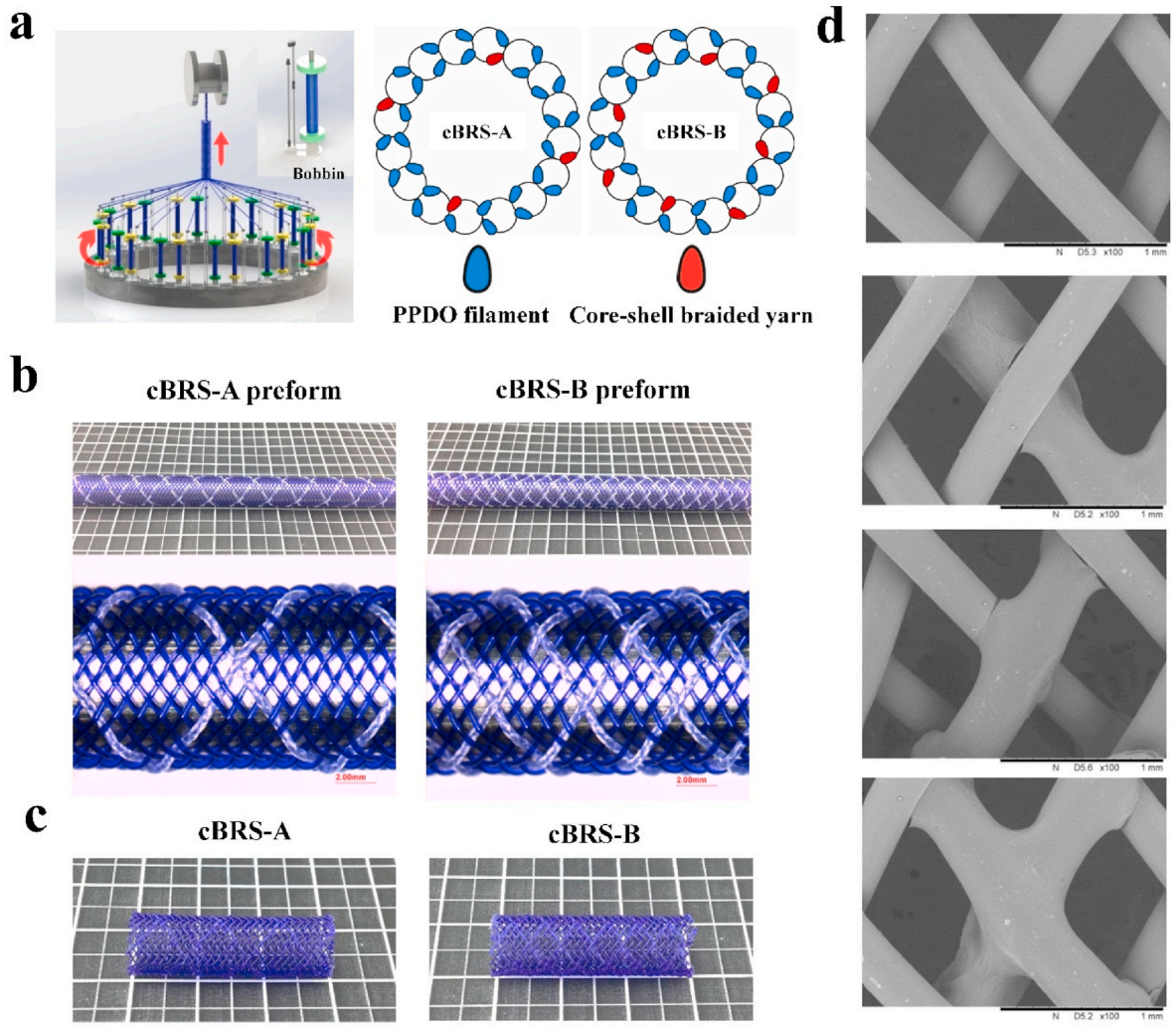

Fig. 3. a. Fabrication of braided cBRSs with different ratios of PPDO monofilaments and PCL/PPDO core-shell composite braided yarns. b. Representative photographs of cBRS preforms before thermal treatment. c. Representative photographs of cBRSs after thermal treatment. d. Representative SEM images of interlacing modes of cBRSs braiding structure.

Table 1
Physical parameters of cBRS-A and cBRS-B.

	Total number of yarns	Number of PPDO	Number of braided yarns	Outer diameter/mm	Braiding angle/°	Pitch/mm
cBRS - A	32	28	4	9.20 ± 0.09	54.88 ± 1.92	18.18 ± 0.42
cBRS - B	32	24	8	9.24 ± 0.13	54.20 ± 1.88	17.76 ± 0.24

Table 2
Proportion of different interlacing modes in cBRSs.

		PPDO-PPDO	PPDO-melted yarn	Melted yarn-melted yarn
Proportion/%	cBRS - A	77.21	20.59	2.20
	cBRS - B	58.33	33.33	8.34

Table 3
Ratio of PPDO and PCL components of cBRSs.

		PPDO	PCL
Proportion/(v/v)%	cBRS - A	88.40	11.60
	cBRS - B	79.13	20.87

by 124.06% and 169.58%, respectively, compared to the typical braids. Besides, by removing all the PPDO monofilament part manually, the residual compression forces of cBRSs were as high as 203.14 ± 25.29 mN/cm and 641.18 ± 57.16 mN/cm for cBRS-A and cBRS-B, suggesting the self-reinforced characteristic of the composite yarns bonding structure (Fig. 4a). The elastic recovery rate of cBRS-B was 94.05 ± 1.60%, which is significantly higher than that of typical control (89.89 ± 1.76%) (Fig. 4b). Moreover, high elasticity and ductility of PCL guaranteed the stability of cBRSs structure, resulted in the minimal mechanical loss during cyclic compression processes for both cBRS-A and cBRS-B (Fig. 4c).

Fig. 4e and f showed the in vitro compliance results of cBRSs and compared typical braids and polyurethane (PU) tubular membrane. As shown in Fig. 4e, cBRS-A was observed with larger change in diameter than that of other groups during the test, indicating its excellent flexibility to conform to pulsatile pressure. In addition, PU tubular

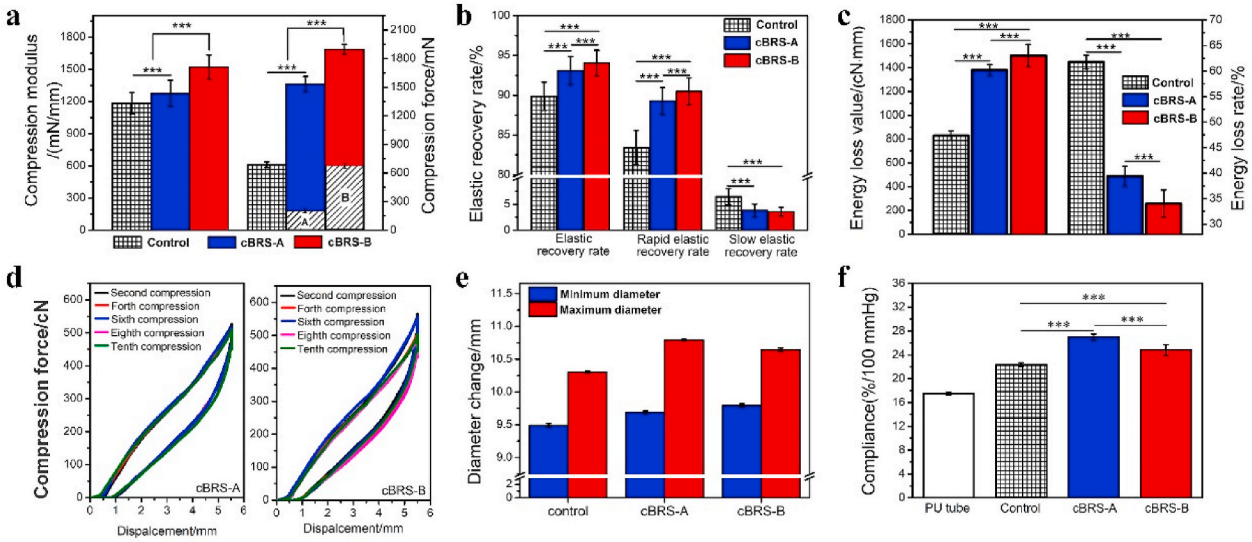

Fig. 4. In vitro mechanical properties of braided cBRSs. a. Compression modulus and compression force of typical braids, cBRS-A and cBRS-B, when they were compressed to half of their initial diameters (n = 3, ***p < 0.005). (A: The compression force of cBRS-A when all PPDO monofilaments were removed from its structure, B: The compression force of cBRS-B when all PPDO monofilaments were removed from its structure). b. Elastic recovery rate, rapid elastic recovery rate and slow elastic recovery rate of typical braids, cBRS-A and cBRS-B, when they were recovered from compression process (n = 3, ***p < 0.005). c. Energy loss value and energy loss rate of typical braids, cBRS-A and cBRS-B during compression and recovery process (n = 3, ***p < 0.005). d. Typical compression load-displacement curves of cBRS-A and cBRS-B when they were cyclically compressed for ten times. e-f. Diameter changes and compliance during 80–120 mmHg pulsatile pressure simulation (n = 3, ***p < 0.005).

membrane has excellent compliance and is commonly used as the positive control to evaluate the compliance of stent graft in vitro [28]. The results also demonstrated better compliance of braided cBRSs than PU tubular membrane, and cBRS-A behaved the best in the flexibility among all groups under physiological pulsatile pressure (Fig. 4f).

3.4. In vitro degradation profile of braided cBRSs

As for the degradation profile of cBRSs in vitro, PPDO monofilaments had higher degradation rate than the core-shell composite yarns during the accelerated degradation test (Fig. 5a). Specifically, struts of the PPDO monofilaments were broken after 30 days, and they were disintegrated and degraded into dissolvable molecules in 50 days. However, for the core-shell composite yarns, the constraint of crossing points remained stable during 50 days degradation, allowing cBRSs with stable structure and good residual mechanical properties. The compression force of cBRS-A remained stable during the first 20 days, while the force increased by 20% in cBRS-B. In contrast, the rapid mechanical loss was observed in the typical control. After that, the loss of compression force in all stents increased continuously in 50-days follow-up, by 41.80 ± 0.16%, 30.69 ± 3.17%, and 64.44 ± 2.53%, for cBRS-A, cBRS-B, and control respectively. The typical control lost the compression force completely in 50 days. For the cBRSs, although the compression forces decreased by 93.37 ± 0.19% and 81.73 ± 0.90% in cBRS-A and cBRS-B, respectively, they remained 30.34 ± 2.72 cN and 100.43 ± 10.60 cN (Fig. 5b).

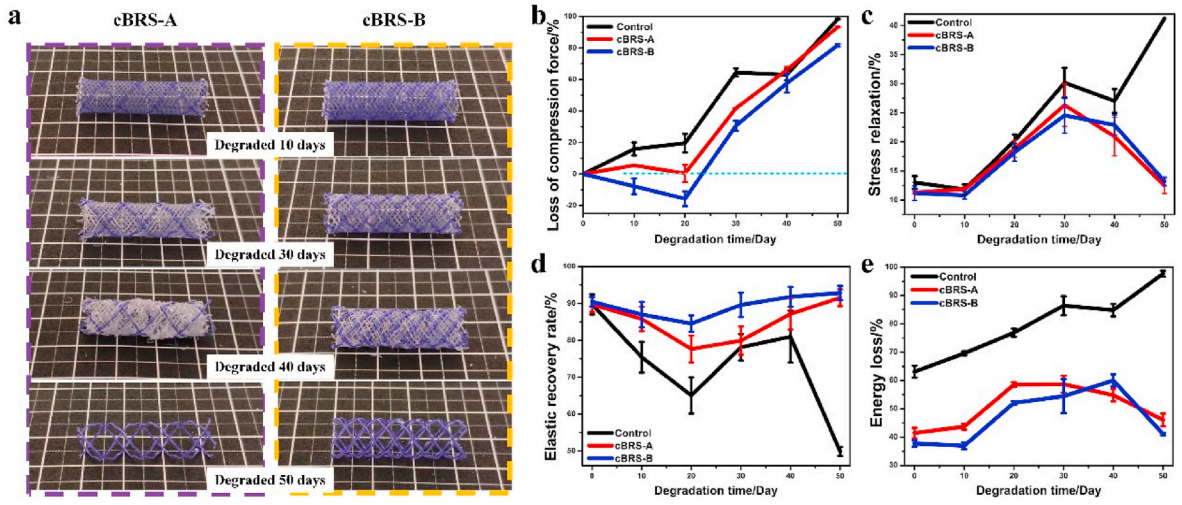

Fig. 5. Degradation evaluation of cBRSs under accelerated in vitro environment. a. Representative macro-photos of cBRS-A and cBRS-B during 50 days degradation. b. Rate of compression force loss of cBRS-A and cBRS-B when they were compressed to half of initial their diameters in different degradation time-points (n = 3). c. Stress relaxation rates of cBRS-A and cBRS-B during compression process in different degradation time-points (n = 3). d. Elastic recovery rates of cBRS-A and cBRS-B during compression-recovery process in different degradation time-points (n = 3). e. Energy loss rates of cBRS-A and cBRS-B during compression-recovery process in different degradation time-points (n = 3).

Stents were compressed to half of their initial diameters and held for 30s, the ratio of compression force loss compared to the highest compression force during compression was calculated and considered as stress relaxation. The results showed that the value in typical braids was continuously increased during degradation, whereas it peaked at 30 days and then recovered thereafter for cBRSs (Fig. 5c). The elastic recovery rate after stent unloading is intuitive to present the recovery ability of braided stents during degradation (Fig. 5d and Supplementary Fig. 2). The elastic recovery rate of control stents were decreased rapidly during degradation. In contrast, the elastic recovery rate remained 75% for cBRS-A and 85% for cBRS-B during the whole hydrolysis process, suggesting the good stabilization of the boding structure of cBRSs. The rate of energy loss during the compression and recovery process exhibited a similar trend with the results of the stress relaxation rate (Fig. 5e).

3.5. Hemocompatibility and cell viability

Although PPDO and PCL have been used in the Food and Drug Administration (FDA) approved medical devices/implants, thermal treatment during composite stents fabrication can change the molecular structure and might lead to poor hemocompatibility and cell toxicity. Fig. 6a and b shows that the hemolysis rates of all samples were well below 1%, which is acceptable for blood-contacting biomaterial use (hemolysis ration lower than 5%). Besides, the cell viability test shows endothelial cell density increased with prolonged culture time, and there is no significant difference observed on day 5 among all groups (Fig. 6c and d). Thus, the effect of the fabrication process in this study is acceptable in terms of biocompatibility.

3.6. In vivo characterization

The surgical procedure and stent implantation were successfully performed with no complications such as implant migration, thrombosis, dissection or aneurism were observed. Since cBRS-A showed better compliance than cBRS-B in vitro, it was selected for in vivo study. All stents (cBRS-A and Wallstent) were implanted in the target vessels of swine, with no signs of intraluminal defects or dissection of the vessel wall. As shown in Fig. 7 a–d, all cBRS stented vessels maintained good patency for 12 months after implantation according to angiograms. The lumen gain percentage of stented vessels in different groups were calculated and showed in Supplementary Fig. 5. The results indicated that the lumen was enlarged immediately after implantation and 1 month follow-up in all groups. After stent implanted for 12 months, the lumen of cBRS stented vessels remained similar area to that in baseline ($-4.60 \pm 4.23\%$ and $-11.44 \pm 3.70\%$), while the lumen narrowed significantly ($-22.54 \pm 4.13\%$) in Wallstent implanted vessels. Images of cBRS explant can also validate the patency of stented vessel (Fig. 7f–h). According to SEM images (Fig. 7i and j), endothelial cells were completely and homogeneously covered on the surface of the stents after 30 days for both cBRS and Wallstent. In 4 months, endothelial cells were organized align to the direction of blood flow (Fig. 8k and l). It indicates low thrombosis risk and good biocompatibility of both cBRS and Wallstent.

A gross morphological evaluation of cBRS explants (Fig. 8a–h) showed the presence of neotissue formation in the lumen after 1 months. A distinct boundary was observed between the neo-tissue and the cBRS suggesting the initiation of neo-tissue formation over the stent followed by integration with the stent struts (Fig. 8a and e). At 4 months, the PPDO monofilaments were distinctively degraded into fragments and replaced with proteoglycan matrix (Fig. 8b and f). After 6 months implantation, the PPDO monofilaments were minimally visible, they were replaced by connective tissue. The granuloma area was also decreased (Fig. 8c and g). In contrast, the core-shell composite yarns were still visible with defined edges, indicating minimal degradation (Fig. 8i–l) [34]. In addition, the degradation scores of the cBRS in abdominal aorta and iliac artery were similar during 12-month follow up (Fig. 8m). We then calculated the lumen area (Fig. 8n) and internal elastic laminal area (Supplementary Fig. 6) of different groups. The lumen area of abdominal aorta after the cBRS implanted slightly decreased from 1 month ($27.90 \pm 1.50\ mm^2$) to 4 months ($24.20 \pm 1.00\ mm^2$), while the lumen enlarged thereafter, possibly due to PPDO component was absorbed after 4 months implantation. Significantly higher lumen area was observed in 12 months ($31.20 \pm 2.20\ mm^2$), indicating the degradation process of the cBRS has minimal impact in vessel healing process. The change of iliac artery lumen area after cBRS implantation performed similar trend

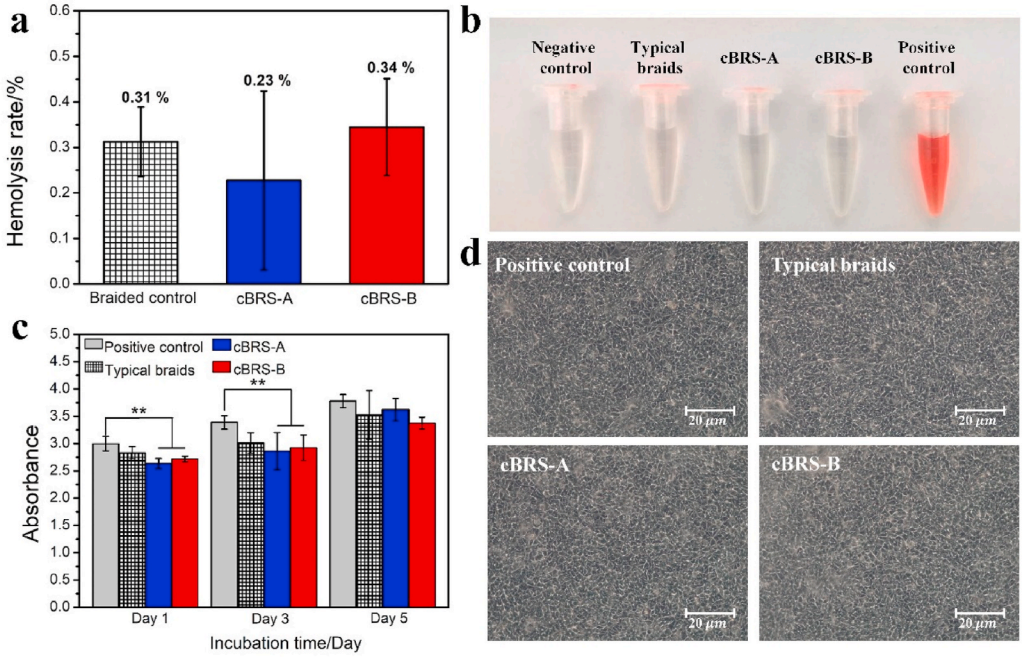

Fig. 6. a–b. Hemolysis rate and optical photos of different groups (n = 3). c. Endothelial cell viability test results of typical braids, cBRS-A and cBRS-B after culturing for 1, 3 and 5 days (n = 3, **p < 0.01). d. Morphology of cells in different groups after cultured for 5 days.

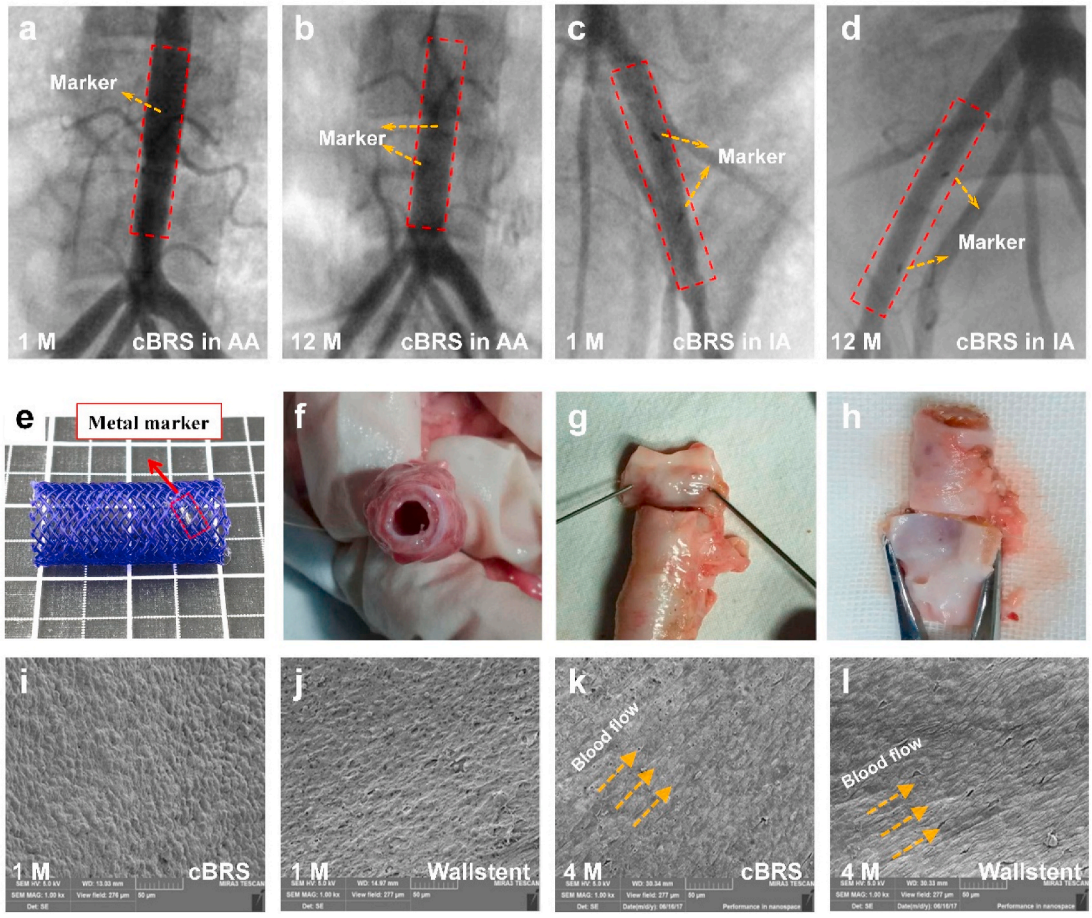

Fig. 7. a–d. Representative angiography images of target vessels after the cBRS implanted for 1 month and 12 months. e. Representative photo of a cBRS-A with metal markers. f–h. Explant of the cBRS after implantation for 2 months. i–l. Representative SEM images of the cBRS and Wallstent explant surfaces after 1 month and 4 month implantation respectively. The surfaces were completely covered by endothelial cells. (AA: Abdominal aorta, IA: Iliac artery).

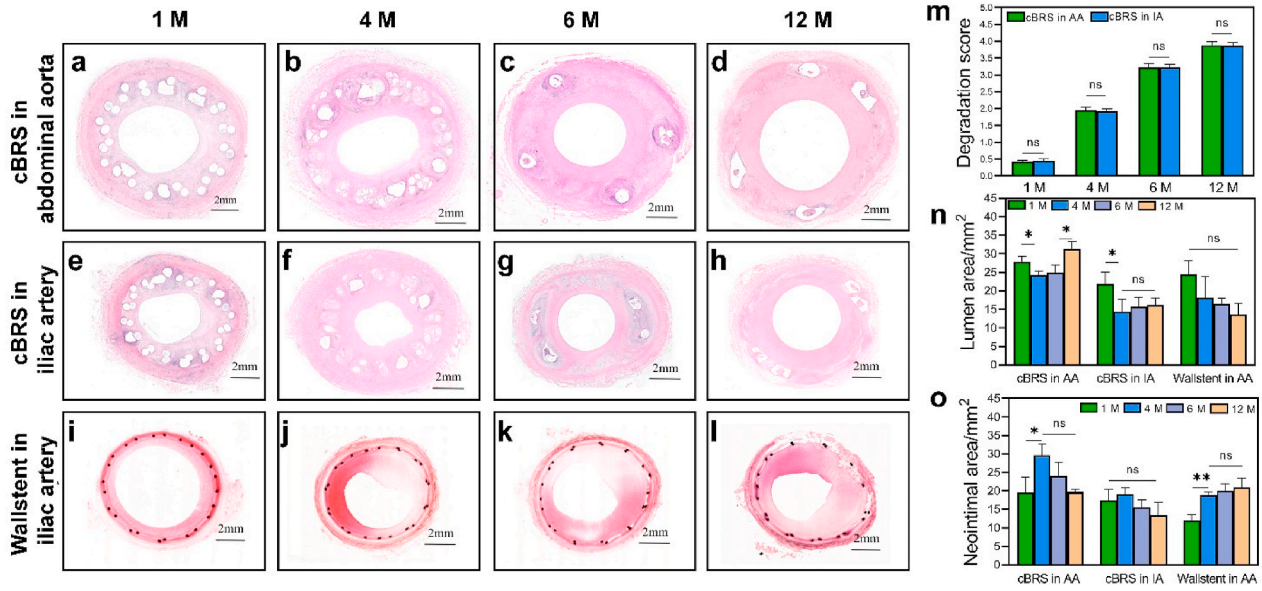

Fig. 8. a–l. Hematoxylin and eosin (H&E) stained images of cBRS and Wallstent implanted vessels during 12 months follow-up. m. Degradation scores of cBRS implanted in abdominal aorta and iliac artery during 12 months follow-up (n = 3, ns: no significant difference). n. Lumen areas of stented vessels during 12 months follow-up, measured from H&E stained images (n = 3, ns: no significant difference, *p < 0.05). o. Neointimal areas of stented vessels during 12 months follow-up, measured and calculated from H&E stained images (n = 3, ns: no significant difference, *p < 0.05, **p < 0.01). For images a-i, vessel lumen is marked as "Lu", cross-section areas of PPDO monofilament and PCL/PPDO composite yarns are marked as "*" and "#", respectively. White arrows showed degradation fragment of PPDO monofilaments in the cBRS.

(Fig. 8n). In contrast, the lumen area of iliac artery implanted with Wallstent decreased continuously in 12-month follow-up (13.70 ± 2.80 mm^2 in 12 months). We also recorded and calculated the changes of neointimal area (Fig. 8o) and neointimal thickness (Supplementary Fig. 7) after the cBRS implanted and compared that with Wallstent stented vessels. Although neointimal area increased from 1 month (19.60 ± 4.2 mm^2 in abdominal aorta and 17.50 ± 3.00 mm^2 in iliac artery) to 4 months (29.60 ± 3.00 mm^2 in abdominal aorta and 19.10 ± 1.70 mm^2 in iliac artery) after cBRS implantation, they decreased constantly after 4 months (12 months: 19.80 ± 0.50 mm^2 in abdominal aorta and 13.40 ± 3.40 mm^2 in iliac artery). However, the neointimal area of vessel after Wallstent implanted increased continuously in 12-month follow-up (1 month: 11.90 ± 1.70 mm^2, 12 months: 20.90 ±0 .50 mm^2).

As shown in Fig. 9a–i, the local tissue showed slight inflammation response to the cBRS after 1 month, 4 month, 6 month and 12 months implantation, similar to that of Wallstent. No tissue necrosis was observed in the neointima and its underlying layers. Macrophages were accumulated around stent struts and gradually engulfed degraded fragments after 4 months implantation [36]. We then calculated the injury score and inflammation score of different groups. Higher injuries were observed in 4 months for cBRS implanted vessels (0.81 ± 0.11 in abdominal aorta, 0.92 ± 0.07 in iliac artery) then other time points. However, in 12 months, the injury scores of cBRS implanted vessels decreased thereafter (0.44 ± 0.05 in abdominal aorta, 0.57 ± 0.05 in iliac artery) and significantly lower than the injury score of Wallstents (0.75 ± 0.08) (Fig. 9j). Besides, although inflammation response is stronger in 4 months (0.70 ± 0.12 in abdominal aorta, 0.76 ± 0.07 in iliac artery) due to mass degradation fragment generation, it remained in mild inflammatory level for both abdominal aorta and iliac artery implanted with the cBRS in 12-month follow-up. The inflammation response of cBRS implanted vessels (score: 0.40 ± 0.05 in abdominal aorta, 0.38 ± 0.03 in iliac artery) were comparable to that of Wallstent implanted vessels (score: 0.31 ± 0.10) after implantation for 12 months (Fig. 9k). As for the histomorphometric area of stenosis, although the in-stent luminal stenosis of cBRS implanted vessels were worse than that of Wallstents in the first month, they showed comparable stenosis ratio in the 4 months. Notably, the stenosis ratio of cBRS stented vessels significantly decreased after the PPDO degradation and continuously decreased in the 12 months follow up (12 months: 38.90 ± 1.30% in abdominal aorta, 45.00 ± 3.20% in iliac artery). In contrast, the Wallstent implanted vessel performed constantly increased stenosis and more than 60% stenosis was observed at 12 months (Fig. 9l).

4. Discussion

Braiding technique has been widely used in fabricating biological tubular devices such as esophageal stent [37], tracheal stent [38], ureteral stent [39], vascular stent [40], and more, owing to the self-expanding property of these devices. Braiding vascular stents behave the advantage over balloon-expandable stents in radial and bending compliance, low risk of vascular injuries. Besides, balloon-expandable devices are unable to re-expand with rapidly growing children vessels. Over-dilatation might result in stent fracture [41,42]. Braiding stents can self-oppose to the vessel wall when expanded to nominal diameter, which is more favorable for pediatric patients [43,44]. Moreover, most of the current BRSs are composed of one component. However, braiding stents can be composed of two or more components, which extends the possibility of customized design for various clinical requirements. In this study, PPDO and PCL were used to fabricate the first generation of braided cBRS. PPDO monofilaments behaved as the main component. Although the elastic modulus of PPDO materials is lower than other bioresorbable polymers, such as poly (L-lactide) (PLLA), poly(lactide-*co*-glycolic acid) (PLGA), it has more suitable degradation time to match the healing process of target vessel. Studies reported that in-stent restenosis process peaked at the third

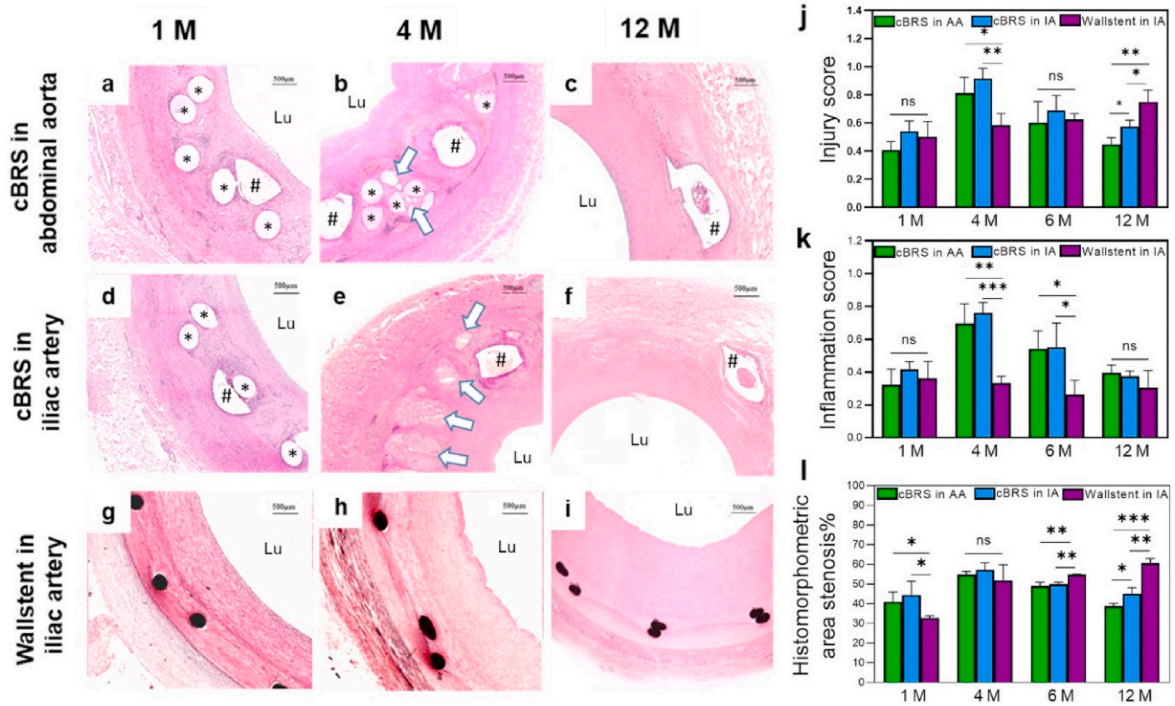

Fig. 9. a–i. Representative high-magnification H&E stained images of cBRS and Wallstent implanted vessels during 12 months follow-up. j. Injury scores of cBRS and Wallstent implanted vessels during 12 months follow-up, recorded from H&E stained images (n = 3, ns: no significant difference, *p < 0.05, **p < 0.01). k. Inflammation scores of cBRS and Wallstent implanted vessels during 12 months follow-up, recorded from H&E stained images (n = 3, ns: no significant difference, *p < 0.05, **p < 0.01, ***p < 0.005). l. cBRS and Wallstent implanted vessels stenosis during 12 months follow-up, calculated from H&E stained images (n = 3, ns: no significant difference, *p < 0.05, **p < 0.01, ***p < 0.005).

month and rarely reached its peak thereafter [45,46]. The remodeling and healing process of diseased vessel can be finished in 6 months. Then, lumen area enlarges from 6 months to 5 years, as reported in most patients after balloon angioplasty [47,48]. Hence, suitable degradation time is crucial for BRS material selection, especially for growing children. The commonly used biomaterial PLLA might be not suitable for pediatric patients since its degradation time is 2–3 years [12,49]. Such a long degradation time can cause similar or even worse long-term thrombosis and restenosis compared to non-degradable metallic stents. It has been reported that PPDO implants are able to maintain mechanical integrity in three months and absorbed entirely in 6 months in aqueous environment [50]. In addition, PPDO implant has been certified by FDA [51], which shows good biocompatibility in vivo in many studies [37,52,53]. Thus, the BRS fabricated by PPDO material can maintain lumen open during vascular healing process with acceptable biocompatibility and suitable degradation time, which is beneficial for patients with congenital heart disease.

Acute stent recoil still limits the application of polymeric BRS. Currently, balloon-expandable polymeric stents are commonly used for vascular stents due to their higher mechanical strength than self-expanding stents. One of the reasons is that balloon expandable stents undergo plastic deformation when they suffered from external force [54]. The plastic deformation is mainly contributed by the crystal region in their molecular structure. However, for braided stents, the movement of crossing yarns and slight elastic deformation of polymers leads to structure deformation. This structural deformation is induced by the molecular chain segments motion of amorphous region in polymer structure, which is significantly easier than the motion in crystallized region of polymer. Thus, the mechanical resistance of typical braided stents is weaker than that of balloon expandable stents. Although it is feasible to use thicker struts to increase mechanical resistance of braided stents, it can be a challenge in deployment process due to their large crossing profile. Several researchers focused on restricting the yarns movement in the crossing points to offer braided stents reinforced mechanical properties. Shin-Horng et al. developed a double opposing helical PLLA stent with several longitudinal fibers glued to the ends of stent [55]. The introduction of these fibers prevented the movement of helical yarns and enhanced its mechanical efficacy. Although their mid-term animal studies showed promising results, the biocompatibility of adhesive glue is still a problem when transfer to clinical use. The early fracture of PLLA struts causing severe restenosis in an infant was also reported [56]. We previously bonded the crossing points of PPDO braided stents with PCL (M.W. 80,000) solution (Supplementary Fig. 3). By using a self-assembled titration device with a capillary nozzle, the PCL solution was dropped on and around the crossing points regularly. After thermally treated under 45 °C for 1 h, PCL was solidified and some crossing points were glued together. The compression force of the stents showed a higher value than the typical braids. However, the adhesion between PCL and PPDO was unstable, resulted in the decrease of compression force in 10-time cyclic compression test. At present, the most successful attempt is reported by 480 Biomedical Inc. [57]. Composite implant was braided with PGLA and coated with poly(glycolide-*co*-caprolactone) elastomer. It has higher mechanical strength compared to braids without elastomer coating, due to the restriction of crossing yarns movement by the coating layer. In this study, we introduced an easier method to facilitate crossing point fixation in braiding structure as described above. The results in this study demonstrated strong peeling force of the bonded crossing yarns and significantly higher mechanical resistance compared to typical braids. The ten times cyclic compression test also indicate good structure stability and durability of the cBRS (Fig. 4d).

Another reason inducing acute stent recoil is the elastic recoil after stent expansion, which depends on material elastic properties and stent structural design. Although balloon-expandable BRS has higher mechanical resistance than typical braids, it is reported with high elastic recoil [58,59]. The laser cutting process in fabricating balloon expandable BRS can cause crack in the laser-affected zones, leading to high stent recoil under cyclic loading [60]. Besides, balloon-expandable BRS is less ductile than metal stents and cannot maintain its strength under persistent external load due to stress relaxation. Irregular plastic deformation of balloon-expandable BRS was reported after crimping process in the PLLA laser-cutting vascular scaffold [61]. The cracks and irregular deformation of balloon expandable stents can lead to stent fracture after deployment [41]. Nevertheless, Dyet et al. [62] reported that self-expanding stents were able to re-expand following deformation. In this study, the cBRS performed good elastic recovery rate (Fig. 4c). The rapid elastic recovery rate of braided stents represents stent ability to recover from deformation immediately. The cBRS exhibited significant higher value (90.48 ± 1.70%) than typical braids (83.41 ± 2.15%). Besides, stents fabricated by polymers commonly behave time-dependent recovery after unloading since they remain in the rubbery or flexible thermoplastic state. This contributes to acute recoil of stents. We analyzed this property by measuring slow elastic recovery rate in this study. The results showed lower values (3.81 ± 1.27% for cBRS-A and 3.57 ± 0.87% for cBRS-B) than that of typical control (6.47 ± 1.56%). The reason might be that less friction need to be conquered and more energy contributes to structure recovery after unloading in the cBRS than that of control stents.

Certainly, the mismatch in vascular compliance after bioresorbable stent implantation is still a severe problem due to the stiffness of BRS, which may cause a disturbance in flow and heterogeneous distribution of wall shear stress. Reports also showed immediate compliance mismatch post-implantation of ABSORB scaffolds [13]. Thus, it is important to design BRS with good elasticity and flexibility to withstand the forces resulting from vessel motion. However, it remains as a challenge for braided stents design since it is controversial to enhance mechanical resistance while maintain their flexibility. The composite implants developed by 480 Biomedical Inc. offered satisfied strength and excellent flexibility by optimizing elastomer branching structure, crosslink density, and molecular weight [57]. In this study, the natural flexibility of typical braids was preserved since not all crossing points were restrained. This offers the cBRS favorable flexibility and compliance compared to PU tubular membrane, which is commonly used to mimic natural vessel during in vitro test.

As mentioned before, degradation profile of BRS is crucial to preserve long-term patency of stented vessel. We evaluated the degradation properties of the cBRS in vitro using accelerated aqueous environment. Our preliminary test demonstrated that the mechanical loss rate of the stent prototypes varied by a factor of 4.67 between 50 °C and 37 °C (Supplementary Fig. 4). Based on the results of degradation test and the correlation between accelerated and real-time resorption, PPDO component of the cBRS is expected to remain mechanical resistance in vitro in approximately 3 months, while core-shell composite yarns remained integrity in 8 months. This result suggests the potential of the cBRS prototypes to meet the clinic requirement. Although PPDO component has faster degradation rate than PCL, cBRS remained good structural stability during degradation, which is benefit from the uniform distribution of the PPDO monofilaments and PCL/PPDL composite yarns. The in vitro degradation results (Fig. 5a) showed that the cBRS remained cylindrical shape and no significant changes occurred in their dimensions when PPDO component degraded entirely. Besides, the elastic recovery rate of cBRS during in vitro degradation process (Fig. 5d) also suggesting the cBRS can remain structural stability and the two-component design of cBRS did not affect the overall efficacy. Besides, BRS is suffered from various mechanical loads after deployment, which has a great impact on the degradation profile of BRS [63]. Our previous in vitro work indicated that the radial force of vessel wall may accelerate the degradation rate of BRS while the overall degradation time was delayed when BRS suffered from pulsatile pressure of blood flow compared to non-loaded BRS [64]. In addition, there is still lack of agreement in terms of the stent-to-artery ratio for polymeric BRS implanted in great vessels. Thus, two vessel positions were selected for

stent implantation in this study, abdominal aorta and iliac artery, due to their different diameters. The diameters of abdominal aorta and iliac artery selected for cBRS implantation were 7.12 ± 0.21 mm and 5.16 ± 0.11 mm, respectively, resulted in the stent-to-artery ratios of 1.13 ± 0.03 and 1.55 ± 0.03. In vivo degradation study showed the both PPDO monofilaments and PCL/PPDO composite yarns of the cBRS remained cross-section integrity in one-month implantation, and the PPDO monofilaments were degraded with some fragments in cross-section in 4 months follow-up. The increasing number of macrophages, fibroblasts and foreign body giant cells around PPDO struts also demonstrated the degradation of PPDO component. This result is consistent with the degradation rate of the cBRS in vitro. In addition, PPDO component was degraded into excessive fragmentation and the region was replaced by the proteoglycan matrix after 6 months. This degradation process occurs earlier than in vitro predicted time. Studies showed that the lysosome in macrophages contributed to the elimination of bioresorbable polymers [65]. The pH of lysosome was reported approximately 5, resulted in acidic environment around PPDO struts [66]. Thus, the degradation process is speculated to be accelerated compared to neutral in vitro aqueous environment. The impact of pulsatile pressure on the degradation rate of the cBRS is considered minimal since the stent struts were entirely covered by endothelial cells after one month. There is no significant difference in the degradation score between stents implanted in abdominal aortas and iliac arteries, also suggesting the minimal influence of external force on the degradation rate of the cBRS (Fig. 8m). Besides the degradation of PPDO component, the PCL/PPDO composite yarns of the cBRS maintained the structure integrity in 12 months follow-up, although the core layer PPDO was replaced by proteoglycan matrix (Fig. 8d and h, Fig. 9c and f). This is also similar to in vitro results. The shell layer of PCL might be degraded in 1–2 years after implantation according to published report [67]. Overall, the cBRS owns two-stage degradation profile after implantation in target arteries. The integrity of the cBRS can be maintained for about 4 months and the main components (88.40% v/v% in cBRS-A) were degraded in 6 months, which is suitable for supporting lumen open in narrowed vessels.

Besides, the two-stage degradation profile is controllable designed in order to reduce the time-specific degradation products concentration, possibly can lighten inflammatory response and further reduce restenosis. Previous studies demonstrated that the inflammatory response is one of the main reasons causing restenosis [68]. It induces proinflammatory cytokines and growth factors generation and subsequently smooth muscle cell migration and proliferation, which results in the neointima over-formation [69]. Currently, anti-inflammatory drugs are commonly used to reduce inflammation reaction, while side effects are reported, such as delayed vascular remodeling process [70,71]. Although the results in this study still showed obvious inflammatory response increasing in 4 months due to partially degradation, it remained in a mild level (Fig. 9k). The stenosis rate is found to be reduced after 4 months and significantly lower than that of Wallstent implantation in 12 months (Fig. 9l). Thus, by introducing more components with suitable while different degradation time, the cBRS are expected to induce lower inflammatory response and probably obtain better long-term patency after implantation than currently developed BRSs.

Although the mid-term in vivo results are promising, we still found the injury score of the cBRS is significantly higher than the composite implant developed by 480 Biomedical Inc. High degree of vessel injury can activate over-growth of neointima. In this study, we found that the injury score was higher in vessel with higher stent-to-artery ratio, although there is no significant difference. It can be explained that higher stent-to-artery ratio leads to higher strain energy stored in compressed stents, which can traumatize the arterial wall. Besides, sharp edge of degradation fragment and the strain energy release during degradation process of the cBRS are expected to contribute to vessel wall injury. It was certified by the results in this study, showing that injury score decreased with degradation products dissolved (Fig. 9j). Moreover, the injury score of PCL/PPDO composite yarns surrounding tissue was significantly higher than that of PPDO yarns (Supplementary Fig. 8). The reason might be that composite yarns have thicker strut than PPDO monofilament, which compressed intima with higher ratio. Also, the surface of composite yarn is not as smooth as PPDO monofilament, inducing more injury to vessel walls (Figs. 2 and 3d). As a result, although the PPDO degraded faster than composite yarn (Supplementary Fig. 9), the inflammation score of composite yarns surrounding tissue was significantly higher than tissue surrounded by PPDO monofilament during 12-month follow-up (Supplementary Fig. 10). Overall, in order to further lower the inflammation response of the cBRS, thinner PCL/PPDO composite yarns with smooth outer surfaces will be used in the future.

5. Study limitations

The profile of the cBRS in this work is still larger than metallic stents and could only be delivered by using an 8 Fr stent delivery system. Thus, it is essential to choose braiding yarns with smaller diameters for cBRS prototype fabrication. It is feasible because of the controllable structural organization of cBRS prototypes, allowing designers to develop cBRS with sufficient mechanical resistance and low stent profile.

6. Conclusion

A novel composite bioresorbable stent, based on braiding technology and thermal treatment, was successfully developed and evaluated with application-relevant measurements of its ability as a cardiovascular stent for pediatric patients. The results in this study demonstrated that the braided cBRS has self-reinforced compression resistance, good flexibility, and suitable degradation profile. Besides, it can be controllable designed to meet complex clinical needs by altering the proportion of different components in the braiding structure. The cBRS also behaved good radial support ability comparable to Wallstent, acceptable biocompatibility and mild inflammation in 12 months in vivo observation. Besides, the cBRS has similar degradation rate when implanted in vessels with different stent-to-artery ratios. Lower crossing profile and thinner stent struts will be used for cBRS fabrication in the near future in order to reduce vessel wall injury.

CRediT authorship contribution statement

Fan Zhao: Conceptualization. **Jing Sun:** Conceptualization. **Wen Xue:** Data curation. **Fujun Wang:** Supervision. **Martin W. King:** Supervision. **Chenglong Yu:** Data curation. **Yongjie Jiao:** Data curation. **Kun Sun:** Supervision. **Lu Wang:** Supervision.

Declaration of competing interest

The authors declare that they have no known competing financial interests or personal relationships that could have appeared to influence the work reported in this paper.

Acknowledgment

F. Zhao and J. Sun contributed equally to this work. The project is supported by the Fundamental Research Funds for the Central Universities (grant No. 2232017A-05, 2232019A3-06), Science and Technology Support Program of Shanghai (grant No. 16441903803, 18441902600), the Chinese Universities Scientific Fund (grant No. CUSF-DH-D-2017012) and 111 project (grant No. B07024).

Appendix A. Supplementary data

Supplementary data to this article can be found online at https://doi.org/10.1016/j.bioactmat.2021.02.017.

References

[1] Y. Li, N.T. Klena, G.C. Gabriel, X. Liu, A.J. Kim, K. Lemke, Y. Chen, B. Chatterjee, W. Devine, R.R. Damerla, Global genetic analysis in mice unveils central role for cilia in congenital heart disease, Nature 521 (7553) (2015) 520–524.

[2] P.A. Schneider, J.R. Laird, G. Tepe, M. Brodmann, T. Zeller, D. Scheinert, C. Metzger, A. Micari, R. Sachar, M.R. Jaff, Treatment effect of drug-coated balloons is durable to 3 years in the femoropopliteal arteries: long-term results of the IN. PACT SFA randomized trial, Circ. Cardiovasc. Interv. 11 (1) (2018), e005891.

[3] F. Alfonso, M.J. Pérez-Vizcayno, J. Cuesta, B.G. del Blanco, A. García-Touchard, J. R. López-Mínguez, M. Masotti, J. Zueco, A. Cequier, M. Velázquez, 3-year clinical follow-up of the RIBS IV clinical trial: a prospective randomized study of drug-eluting balloons versus everolimus-eluting stents in patients with in-stent restenosis in coronary arteries previously treated with drug-eluting stents, JACC-Cardiovasc. Interv. 11 (10) (2018) 981–991.

[4] J. Torrado, L. Buckley, A. Durán, P. Trujillo, S. Toldo, J.V. Raleigh, A. Abbate, G. Biondi-Zoccai, L.A. Guzmán, Restenosis, stent thrombosis, and bleeding complications: navigating between Scylla and Charybdis, J. Am. Coll. Cardiol. 71 (15) (2018) 1676–1695.

[5] Y. Sotomi, Y. Onuma, C. Collet, E. Tenekecioglu, R. Virmani, N.S. Kleiman, P. W. Serruys, Bioresorbable scaffold: the emerging reality and future directions, Circ. Res. 120 (8) (2017) 1341–1352.

[6] S. Bangalore, H.G. Bezerra, D.G. Rizik, E.J. Armstrong, B. Samuels, S.S. Naidu, C. L. Grines, M.T. Foster, J.W. Choi, B.D. Bertolet, The state of the absorb bioresorbable scaffold: consensus from an expert panel, JACC Cardiovasc. Interv. 10 (23) (2017) 2349–2359.

[7] J.A. Ormiston, F. De Vroey, P.W. Serruys, M.W. Webster, Bioresorbable polymeric vascular scaffolds: a cautionary tale, Circ. Cardiovasc. Interv. 4 (5) (2011) 535–538.

[8] N. Moriyama, K. Shishido, Y. Tanaka, S. Yokota, T. Hayashi, H. Miyashita, T. Koike, H. Yokoyama, T. Takada, T. Nishimoto, Neoatherosclerosis 5 years after bioresorbable vascular scaffold implantation, J. Am. Coll. Cardiol. 71 (17) (2018) 1882–1893.

[9] A. Abizaid, R.A. Costa, J. Schofer, J. Ormiston, M. Maeng, B. Witzenbichler, R. V. Botelho, J.R. Costa, D. Chamié, A.S. Abizaid, Serial multimodality imaging and 2-year clinical outcomes of the novel DESolve novolimus-eluting bioresorbable coronary scaffold system for the treatment of single de novo coronary lesions, JACC-Cardiovasc. Interv. 9 (6) (2016) 565–574.

[10] A. Abizaid, D. Carrié, N. Frey, M. Lutz, J. Weber-Albers, D. Dudek, B. Chevalier, S.-C. Weng, R.A. Costa, J. Anderson, 6-month clinical and angiographic outcomes of a novel radiopaque sirolimus-eluting bioresorbable vascular scaffold: the FANTOM II study, JACC Cardiovasc. Interv. 10 (18) (2017) 1832–1838.

[11] J.J. Wykrzykowska, R.P. Kraak, S.H. Hofma, R.J. van der Schaaf, E.K. Arkenbout, A.J. IJsselmuiden, J. Elias, I.M. van Dongen, R.Y. Tijssen, K.T. Koch, Bioresorbable scaffolds versus metallic stents in routine PCI, N. Engl. J. Med. 376 (24) (2017) 2319–2328.

[12] D.J. Kereiakes, S.G. Ellis, C. Metzger, R.P. Caputo, D.G. Rizik, P.S. Teirstein, M. R. Litt, A. Kini, A. Kabour, S.O. Marx, 3-year clinical outcomes with everolimus-eluting bioresorbable coronary scaffolds: the ABSORB III trial, J. Am. Coll. Cardiol. 70 (23) (2017) 2852–2862.

[13] P.J. Wang, N. Ferralis, C. Conway, J.C. Grossman, E.R. Edelman, Strain-induced accelerated asymmetric spatial degradation of polymeric vascular scaffolds, Proc. Natl. Acad. Sci. U. S. A. 115 (11) (2018) 2640–2645.

[14] B. Chevalier, A. Cequier, D. Dudek, M. Haude, D. Carrie, M. Sabaté, S. Windecker, S. Reith, M. de Sousa Almeida, G. Campo, A. Iniguez, Four-year follow-up of the randomised comparison between an everolimus-eluting bioresorbable scaffold and an everolimus-eluting metallic stent for the treatment of coronary artery stenosis (ABSORB II Trial), EuroIntervention 13 (2018) 1561–1564.

[15] R.A. Byrne, G.W. Stone, J. Ormiston, A. Kastrati, Coronary balloon angioplasty, stents, and scaffolds, Lancet 390 (10096) (2017) 781–792.

[16] B. Tesfamariam, Bioresorbable vascular scaffolds: biodegradation, drug delivery and vascular remodeling, Pharmacol. Res. 107 (2016) 163–171.

[17] C. Collet, R.J. de Winter, Y. Onuma, P.W. Serruys, The Absorb bioresorbable vascular scaffold for the treatment of coronary artery disease, Expert Opin. Drug Deliv. 13 (10) (2016) 1489–1499.

[18] J. Iqbal, Y. Onuma, J. Ormiston, A. Abizaid, R. Waksman, P. Serruys, Bioresorbable scaffolds: rationale, current status, challenges, and future, Eur. Heart J. 35 (12) (2014) 765–776.

[19] Y. Zhang, C.V. Bourantas, V. Farooq, T. Muramatsu, R. Diletti, Y. Onuma, H. M. Garcia-Garcia, P.W. Serruys, Bioresorbable scaffolds in the treatment of coronary artery disease, Med. Dev. (Auckland, NZ) 6 (2013) 37.

[20] T.R. Welch, A.W. Nugent, S.R.V. Veeram, Biodegradable Stents for Congenital Heart Disease. Congenital Heart Disease Intervention, an Issue of Interventional Cardiology Clinics, Ebook; Elsevier, Philadelphia, PA, USA, 2018, p. 81.

[21] R.D. Alexy, D.S. Levi, Materials and manufacturing technologies available for production of a pediatric bioabsorbable stent, Biomed Res. Int. 2013 (2013).

[22] F. Zhao, W. Xue, F. Wang, J. Sun, J. Lin, L. Liu, K. Sun, L. Wang, Braided bioresorbable cardiovascular stents mechanically reinforced by axial runners, J. Mech. Behav. Biomed. Mater. 89 (2019) 19–32.

[23] J.S. Soares, K.R. Rajagopal, J.E. Moore, Deformation-induced hydrolysis of a degradable polymeric cylindrical annulus, Biomech. Model. Mechanobiol. 9 (2) (2010) 177–186.

[24] C. Shanahan, S.A. Tofail, P. Tiernan, Viscoelastic braided stent: finite element modelling and validation of crimping behaviour, Mater. Des. 121 (2017) 143–153.

[25] F. Zhao, W. Xue, F. Wang, C. Yu, H. Xu, Y. Hao, L. Wang, A new approach to improve the local compressive properties of PPDO self-expandable stent, J. Mech. Behav. Biomed. Mater. 68 (2017) 318–326.

[26] C.R. Wang, P.H. Zhang, In vitro degradation behaviours of PDO monofilament and its intravascular stents with braided structure, Autex Res. J. 16 (2) (2016) 80–89.

[27] X. Chen, D. Hou, L. Wang, Q. Zhang, J. Zou, G. Sun, Antibacterial surgical silk sutures using a high-performance slow-release carrier coating system, ACS Appl. Mater. Interfaces 7 (40) (2015) 22394–22403.

[28] Y. Guan, L. Wang, J. Lin, M.W. King, Compliance study of endovascular stent grafts incorporated with polyester and polyurethane graft materials in both stented and unstented zones, Materials 9 (8) (2016) 658.

[29] B.A. Boe, J.D. Zampi, K.R. Schumacher, S. Yu, A.K. Armstrong, The use and outcomes of small, medium and large premounted stents in pediatric and congenital heart disease, Pediatr. Cardiol. 37 (8) (2016) 1525–1533.

[30] R. Kornowski, M.K. Hong, F.O. Tio, O. Bramwell, H. Wu, M.B. Leon, In-stent restenosis: contributions of inflammatory responses and arterial injury to neointimal hyperplasia, J. Am. Coll. Cardiol. 31 (1) (1998) 224–230.

[31] E.L. Hedberg, H.C. Kroese-Deutman, C.K. Shih, R.S. Crowther, D.H. Carney, A. G. Mikos, J.A. Jansen, In Vivo degradation of porous poly (propylene fumarate)/poly (DL-lactic-co-glycolic acid) composite scaffolds, Biomaterials 26 (22) (2005) 4616–4623.

[32] T.D. Kozai, K. Catt, X. Li, Z.V. Gugel, V.T. Olafsson, A.L. Vazquez, X.T. Cui, Mechanical failure modes of chronically implanted planar silicon-based neural probes for laminar recording, Biomaterials 37 (2015) 25–39.

[33] S.H. Im, C.Y. Kim, Y. Jung, Y. Jang, S.H. Kim, Biodegradable vascular stents with high tensile and compressive strength: a novel strategy for applying monofilaments via solid-state drawing and shaped-annealing processes, Biomater. Sci. 5 (3) (2017) 422–431.

[34] L.H. Chan-Chan, R. Solis-Correa, R.F. Vargas-Coronado, J.M. Cervantes-Uc, J. Cauich-Rodríguez, P. Quintana, P. Bartolo-Pérez, Degradation studies on segmented polyurethanes prepared with HMDI, PCL and different chain extenders, Acta Biomater. 6 (6) (2010) 2035–2044.

[35] Y. Zhu, K. Yang, R. Cheng, Y. Xiang, T. Yuan, Y. Cheng, B. Sarmento, W. Cui, The current status of biodegradable stent to treat benign luminal disease, Mater. Today 20 (9) (2017) 516–529.

[36] J. Sun, K. Sun, K. Bai, S. Chen, F. Zhao, F. Wang, N. Hong, H. Hu, Oversized composite braided biodegradable stents with post-dilatation for pediatric applications: mid-term results of a porcine study, Biomater. Sci. 8 (18) (2020) 5183–5195 (Reproduced by permission of The Royal Society of Chemistry).

[37] A. Repici, F.P. Vleggaar, C. Hassan, P.G. Van Boeckel, F. Romeo, N. Pagano, A. Malesci, P.D. Siersema, Efficacy and safety of biodegradable stents for refractory benign esophageal strictures: the BEST (Biodegradable Esophageal Stent) study, Gastrointest. Endosc. 72 (5) (2010) 927–934.

[38] L. Novotny, M. Crha, P. Rauser, A. Hep, J. Misik, A. Necas, D. Vondrys, Novel biodegradable polydioxanone stents in a rabbit airway model, J. Thorac. Cardiovasc. Surg. 143 (2) (2012) 437–444.

[39] T. Zou, L. Wang, W. Li, W. Wang, F. Chen, M.W. King, A resorbable bicomponent braided ureteral stent with improved mechanical performance, J. Mech. Behav. Biomed. Mater. 38 (2014) 17–25.

[40] C.R. Wang, P.H. Zhang, Design and characterization of PDO biodegradable intravascular stents, Text. Res. J. 87 (16) (2016) 1968–1976.

[41] Q. Luo, X. Liu, Z. Li, C. Huang, W. Zhang, J. Meng, Z. Chang, Z. Hua, Degradation model of bioabsorbable cardiovascular stents, PloS One 9 (11) (2014), e110278.

[42] R.V. Marrey, R. Burgermeister, R.B. Grishaber, R. Ritchie, Fatigue and life prediction for cobalt-chromium stents: a fracture mechanics analysis, Biomaterials 27 (9) (2006) 1988–2000.

[43] D.J. Clark, S. Lessio, M. O'Donoghue, C. Tsalamandris, R. Schainfeld, K. Rosenfield, Mechanisms and predictors of carotid artery stent restenosis: a serial intravascular ultrasound study, J. Am. Coll. Cardiol. 47 (12) (2006) 2390–2396.

[44] H. Krankenberg, T. Zeller, M. Ingwersen, J. Schmalstieg, H.M. Gissler, S. Nikol, I. Baumgartner, N. Diehm, E. Nickling, S. Muller-Hulsbeck, R. Schmiedel, G. Torsello, W. Hochholzer, C. Stelzner, K. Brechtel, W. Ito, R. Kickuth, E. Blessing, M. Thieme, J. Nakonieczny, T. Nolte, R. Gareis, H. Boden, S. Sixt, Self-expanding versus balloon-expandable stents for iliac artery occlusive disease: the randomized ICE trial, JACC Cardiovasc. Interv. 10 (16) (2017) 1694–1704.

[45] T. Kimura, S. Kaburagi, T. Tamura, H. Yokoi, Y. Nakagawa, H. Yokoi, N. Hamasaki, H. Nosaka, M. Nobuyoshi, G.S. Mintz, Remodeling of human coronary arteries undergoing coronary angioplasty or atherectomy, Circulation 96 (2) (1997) 475–483.

[46] T. Kimura, H. Yokoi, Y. Nakagawa, T. Tamura, S. Kaburagi, Y. Sawada, Y. Sato, H. Yokoi, N. Hamasaki, H. Nosaka, Three-year follow-up after implantation of metallic coronary-artery stents, N. Engl. J. Med. 334 (9) (1996) 561–567.

[47] R. Erbel, C. Di Mario, J. Bartunek, J. Bonnier, B. de Bruyne, F.R. Eberli, P. Erne, M. Haude, B. Heublein, M. Horrigan, C. Ilsley, D. Böse, J. Koolen, T.F. Lüscher, N. Weissman, R. Waksman, Temporary scaffolding of coronary arteries with bioabsorbable magnesium stents: a prospective, non-randomised multicentre trial, Lancet 369 (9576) (2007) 1869–1875.

[48] J.A. Ormiston, F.M. Stewart, A.H. Roche, B.J. Webber, R.M. Whitlock, M. W. Webster, Late regression of the dilated site after coronary angioplasty: a 5-year quantitative angiographic study, Circulation 96 (2) (1997) 468–474.

[49] C.M. Campos, Y. Ishibashi, J. Eggermont, S. Nakatani, Y.K. Cho, J. Dijkstra, J. H. Reiber, A. Sheehy, J. Lane, M. Kamberi, Echogenicity as a surrogate for bioresorbable everolimus-eluting scaffold degradation: analysis at 1-, 3-, 6-, 12-18, 24-, 30-, 36-and 42-month follow-up in a porcine model, Int. J. Cardiovasc. Imaging 31 (3) (2015) 471–482.

[50] H.L. Lin, C. Chu, D. Grubb, Hydrolytic degradation and morphologic study of poly-p-dioxanone, J. Biomed. Mater. Res. 27 (2) (1993) 153–166.
[51] M.A. Sabino, S. González, L. Márquez, J.L. Feijoo, Study of the hydrolytic degradation of polydioxanone PPDX, Polym. Degrad. Stabil. 69 (2) (2000) 209–216.
[52] S.H. Dayan, N. Ashourian, Polydioxanone absorbable plate for cartilaginous grafting in endonasal rhinoplasty: a randomized clinical trial, JAMA Facial Plast. Surg. 18 (1) (2016) 47–53.
[53] J.A. Martins, A.A. Lach, H.L. Morris, A.J. Carr, P.-A. Mouthuy, Polydioxanone implants: a systematic review on safety and performance in patients, J. Biomater. Appl. 34 (7) (2020) 902–916.
[54] Q. Wang, G. Fang, Y. Zhao, G. Wang, T. Cai, Computational and experimental investigation into mechanical performances of Poly-L-Lactide Acid (PLLA) coronary stents, J. Mech. Behav. Biomed. Mater. 65 (2017) 415–427.
[55] T.R. Welch, R.C. Eberhart, S.V. Reddy, J. Wang, A. Nugent, J. Forbess, Novel bioresorbable stent design and fabrication: congenital heart disease applications, Cardiovasc. Eng. Technol. 4 (2) (2013) 171–182.
[56] B. McCrossan, C. McMahon, K. Walsh, First reported use of drug-eluting bioabsorbable vascular scaffold in congenital heart disease, Catheter Cardiovasc. Interv. 87 (2) (2016) 324–328.
[57] U. Sharma, D. Concagh, L. Core, Y. Kuang, C. You, Q. Pham, G. Zugates, R. Busold, S. Webber, J. Merlo, The development of bioresorbable composite polymeric implants with high mechanical strength, Nat. Mater. 17 (1) (2018) 96–103.
[58] A. Schiavone, L. Zhao, A.A. Abdel-Wahab, Effects of material, coating, design and plaque composition on stent deployment inside a stenotic artery-finite element simulation, Mater. Sci. Eng. C 42 (2014) 479–488.
[59] A. Schiavone, L. Zhao, A computational study of stent performance by considering vessel anisotropy and residual stresses, Mater. Sci. Eng. C 62 (2016) 307–316.
[60] W. Schmidt, P. Behrens, C. Brandt-Wunderlich, S. Siewert, N. Grabow, K.-P. Schmitz, In vitro performance investigation of bioresorbable scaffolds–standard tests for vascular stents and beyond, Cardio. Revasc. Med. 17 (6) (2016) 375–383.
[61] A. Ailianou, K. Ramachandran, M.B. Kossuth, J.P. Oberhauser, J.A. Kornfield, Multiplicity of morphologies in poly (l-lactide) bioresorbable vascular scaffolds, Proc. Natl. Acad. Sci. U. S. A. 113 (42) (2016) 11670–11675.
[62] J.F. Dyet, W.G. Watts, D.F. Ettles, A.A. Nicholson, Mechanical properties of metallic stents: how do these properties influence the choice of stent for specific lesions? Cardiovasc. Intervent. Radiol. 23 (1) (2000) 47–54.
[63] Y. Li, Z. Chu, X. Li, X. Ding, M. Guo, H. Zhao, J. Yao, L. Wang, Q. Cai, Y. Fan, The effect of mechanical loads on the degradation of aliphatic biodegradable polyesters, Regen. Biomater. 4 (3) (2017) 179–190.
[64] F. Zhao, F. Wang, M.W. King, L. Wang, Effect of dynamic and static loading during in vitro degradation of a braided composite bioresorbable cardiovascular stent, Mater. Lett. 250 (2019) 12–15.
[65] J.M. Anderson, A. Rodriguez, D.T. Chang, Foreign body reaction to biomaterials, Semin. Immunol. (2008) 86–100.
[66] M. Lundborg, R. Falk, A. Johansson, W. Kreyling, P. Camner, Phagolysosomal pH and dissolution of cobalt oxide particles by alveolar macrophages, Environ. Health Perspect. 97 (1992) 153–157.
[67] S. de Valence, J.-C. Tille, D. Mugnai, W. Mrowczynski, R. Gurny, M. Möller, B. H. Walpoth, Long term performance of polycaprolactone vascular grafts in a rat abdominal aorta replacement model, Biomaterials 33 (1) (2012) 38–47.
[68] T. Inoue, K. Croce, T. Morooka, M. Sakuma, K. Node, D.I. Simon, Vascular inflammation and repair: implications for re-endothelialization, restenosis, and stent thrombosis, JACC-Cardiovasc. Interv. 4 (10) (2011) 1057–1066.
[69] M. Maleknia, N. Ansari, H. Haybar, M. Maniati, N. Saki, Inflammatory growth factors and in-stent restenosis: effect of cytokines and growth factors, SN CCM (2020) 1–11.
[70] H.M. Nef, J. Wiebe, N. Foin, F. Blachutzik, O. Dörr, S. Toyloy, C.W. Hamm, A new novolimus-eluting bioresorbable coronary scaffold: present status and future clinical perspectives, Int. J. Cardiol. 227 (2017) 127–133.
[71] S. Verheye, J.A. Ormiston, J. Stewart, M. Webster, E. Sanidas, R. Costa, J.R. Costa, D. Chamie, A.S. Abizaid, I. Pinto, A next-generation bioresorbable coronary scaffold system: from bench to first clinical evaluation: 6-and 12-month clinical and multimodality imaging results, JACC Cardiovasc. Interv. 7 (1) (2014) 89–99.